Catalytic mechanism of aldose reductase studied by the combined potentials of quantum mechanics and molecular mechanics

Yong S. Lee [a,*], Milan Hodoscek [b,c], Bernard R. Brooks [b], Peter F. Kador [a]

[a] *National Eye Institute, National Institutes of Health, Bethesda, MD 20892, USA*
[b] *Laboratory of Structural Biology, DCRT, National Institutes of Health, Bethesda, MD 20892, USA*
[c] *National Institute of Chemistry, Ljubljana, Slovenia*

Abstract

The catalytic reduction of D-glyceraldehyde to glycerol by aldose reductase has been investigated with the combined potentials of quantum mechanics (QM) and molecular mechanics (MM) to resolve the question of whether Tyr48 or His110 serves as the proton donor during catalysis. Site directed mutagenesis studies favor Tyr48 as the proton donor while the presence of a water channel linking the $N\delta 1$ of His110 to the bulk solvent suggests that His110 is the proton donor. Utilizing the combined potentials of QM and MM, the binding mode of substrate D-glyceraldehyde was investigated by optimizing the local geometry of Asp43, Lys77, Tyr48, His110 and NADPH at the active site of aldose reductase. Reaction pathways for the reduction of D-glyceraldehyde to glycerol were then constructed by treating both Tyr48 and His110 as proton donors. Comparison of energetics obtained from the reaction pathways suggests His110 to be the proton donor. Based on these findings, a reduction mechanism of D-glyceraldehyde to glycerol is described. © 1998 Elsevier Science B.V.

1. Introduction

Aldose reductase (E.C. 1.1.1.21; AR) is an enzyme which utilizes NADPH to reduce the aldehyde form of glucose to sorbitol in the polyol pathway. AR has been linked to diabetes-associated structural and/or functional changes of peripheral nerves, lens, retina, cornea, iris and kidney [1,2]. The reduction of an aldehyde substrate to an alcohol by AR consists of a *4-pro-R* hydride transfer from the coenzyme NADPH and a proton transfer from one of the amino acid residues in the active site to the substrate.

Recently solved crystal structures of AR [3–5] have spurred great interest in elucidating the catalytic mechanism of AR at the atomic level. Fig. 1 illustrates the catalytic site of AR comprising Tyr48, His110, Cys298 and the nicotinamide ring of the NADPH. Tyr48, His110 and Cys298 are all positioned to function as a potential proton donor during catalysis; however, the proton source in conjunction with the hydride transfer process remains controversial.

* Corresponding author. NEI/NIH Bldg. 10 RM 10B11, Bethesda, MD 20892, USA. Tel. +1-301-496-8548; fax: +1-301-402-2399; e-mail: yongslee@helix.nih.gov
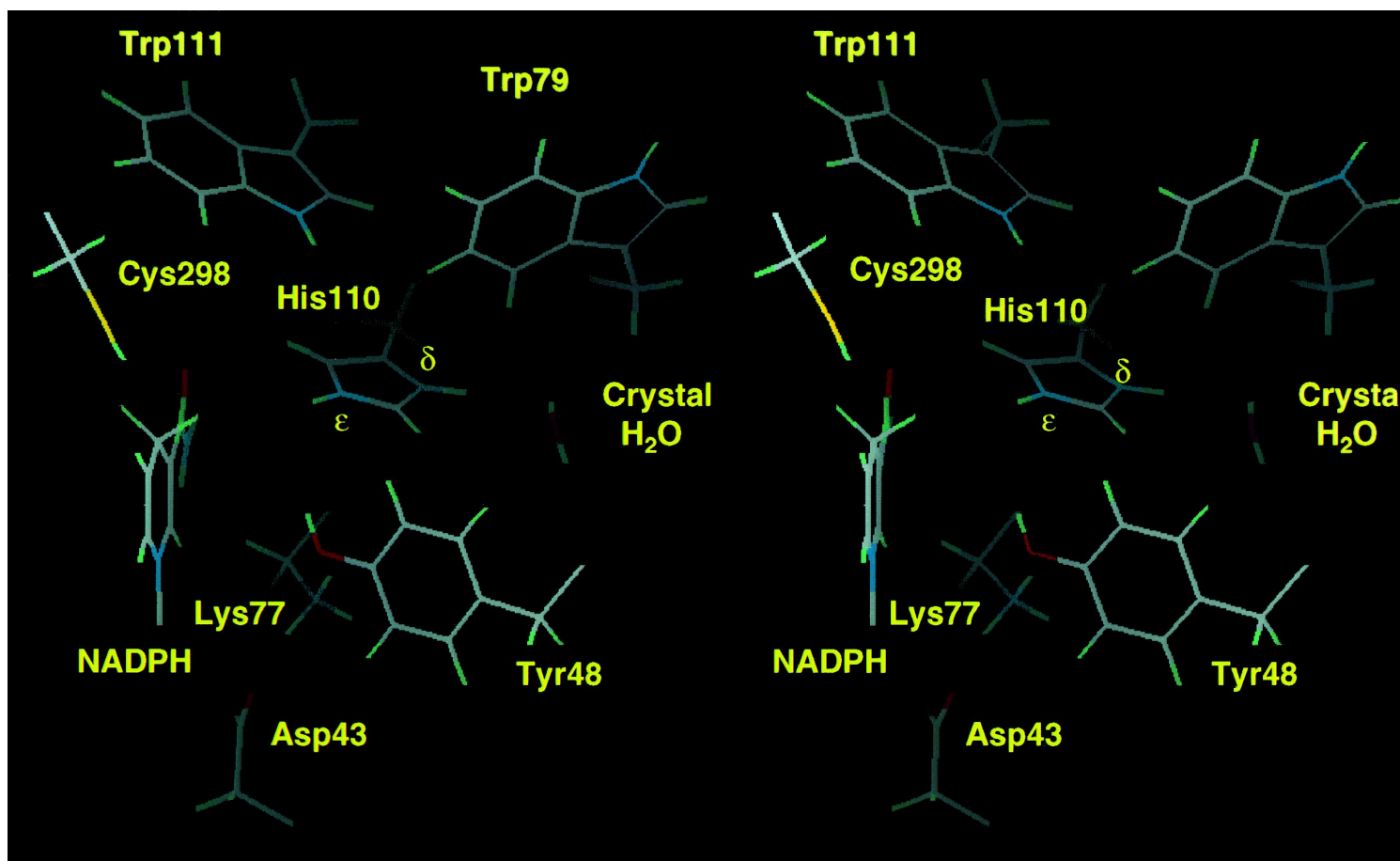
Fig. 1. Stereo view of the catalytic site of human aldose reductase. Shown are the amino acid residues and the nicotinamide ring of the NADPH at the active site. A crystal water linking the Nδ1 of His110 to the bulk solvent is shown. The HBUILD routine of CHARMM was utilized to add hydrogens to the amino acid residues of the human aldose reductase complexed with the NADPH (1ADS, the Brookhaven Protein Data Bank). His110 was protonated.

Site directed mutagenesis studies of human AR [6,7] indicate that there is a complete loss of enzymatic activity when Tyr48 was mutated to phenylalanine (Y48F). In contrast, the mutation of His110 to asparagine (H110N) resulted in ca. 10^6 fold decrease in catalytic efficiency (k_{cat}/K_m) measured with D-glyceraldehyde as substrate [6]. The replacement of His110 with glutamine (H110Q) and alanine (H110A) resulted in a 1000 to 20,000-fold decrease in the k_{cat}/K_m, respectively for the reduction of DL-glyceraldehyde [7]. Strong reductase activity was maintained by both alanine and serine mutants at Cys298 [6,8]. Based on these findings, Tyr48 rather than His110 was concluded to be the proton donor. Recent kinetic studies with human AR also favor Tyr48 as the proton donor [9–11]. Although the pK_a of Tyr (ca. 10) is much higher than that of protonated His (ca. 6–7), a positively charged neighboring Lys77 has been proposed to lower the pK_a of Tyr48 through stabilization of a tyrosinate anion by a salt bridge formation [6,7,12]. The hydrophobic environment surrounding His110 has been claimed to favor a neutral His110 rather than a protonated His110 [6,7,12]. Molecular modeling calculations on the binding of sugar substrates to human AR also indicate that a neutral His110 with the N$\varepsilon 2$ hydrogen is favored when the sugar substrates are bound to the complex of AR with NADPH [13]. His110, in contrast, has been proposed to be the proton source in investigations of the pH-dependence of alcohol oxidation by bovine lens AR [14,15] which indicate that an ionizable group with a pK_a of 6.5–7 is present at the active site. This conclusion is supported by the recent crystal structure of pig lens AR [16] which reveals the existence of a water channel between the N$\delta 1$ of His110 and the bulk solvent. This water channel (Fig. 1), which is also conserved in the crystal structure of human AR [4,5] and the Y48H mutant [7], has been claimed to stabilize the protonated form of His110.

Asp43, Lys77 and His110 are strictly conserved among the known members of the aldo-keto oxidase superfamily while Tyr48 is conserved in all but the Japanese bull frog ρ-crystalline [6]. Of these four residues, Lys77 forms a hydrogen bond with Tyr48 that is assumed to serve as a general acid–base catalyst for a number of proteins in the aldo-keto oxidase superfamily. These include 3α-hydroxy-steroid dehydrogenase [17], aldehyde reductase [18,19] and AR [6,7,20–22]. To gain insight into the roles of these critical amino acids at the active site, combined quantum mechanical and molecular mechanical studies have been conducted with the substrate D-glyceraldehyde docked into the active site. These studies included the construction of potential energy surface of the reduction process.

2. Method

2.1. Combined potentials of quantum mechanics and molecular mechanics

While ideally investigations of the structure and energetics of proteins should be conducted by treating all atoms quantum mechanically, the large number of atoms to be included in calculations make this method inappropriate at present. Therefore, a combined QM/MM method was utilized to study the structure and energetics of proteins at the ab initio level where GAMESS [23] has been interfaced with CHARMM [24]. The present QM/MM approach [25] is conceptually similar to other QM/MM methods developed for the investigation of chemical reactions in enzymes [26–29] and in solution [30–32] but differs in its implementation. In the QM/MM method, the active site of a protein is partitioned into a small region which is modeled with ab initio methods using GAMESS. The bulk of the protein and the protein environment are treated classically by CHARMM, and an interaction potential is applied to properly interface the distinct models [25]. This tool allows for the treatment of atoms at the active site at the ab initio level with various basis sets while explicitly including atoms outside the active site at the MM level. Energetics from GAMESS/CHARMM [25] include all QM energy terms for QM atoms, all MM energy terms for MM atoms, and QM/MM terms such as Van der Waals and electrostatic energy between QM and MM atoms as well as appropriate classical energy terms to properly treat connectivity between QM and MM atoms.

2.2. Docking D-glyceraldehyde into the active site of AR and partitioning the active site into QM and MM regions

Human AR complexed with cofactor and crystal waters (1ADS) [4] were obtained from the Brookhaven Protein Data Bank. Hydrogens were added to the amino acid residues of human AR using the HBUILD routine of CHARMM [24]. To ensure that the *re* face of the carbonyl of D-glyceraldehyde receives the hydride from the NADPH, the carbonyl oxygen of D-glyceraldehyde was positioned within the distance of hydrogen bonding interactions with the $N\varepsilon 2$ hydrogen of His110 and the hydroxyl of Tyr48. Crystal water molecules and citrate [5] overlapping D-glyceraldehyde at the active site were removed. SCF calculations with the 6-31G* basis [33] set were performed to assign partial charges to the NADPH and D-glyceraldehyde. For all histidine residues in AR except His110, hydrogens were assigned to the $N\delta 1$ of neutral histidine. His110 was assumed to be positively charged. All Asp and Glu residues were assumed to be negatively charged while Arg and Lys were positively charged. The complex (AR–NADPH–Crystal H_2Os–D-glyceraldehyde) was assumed to carry a net charge of -5 (-1 for AR and -4 for NADPH). This complex was further hydrated by placing it into a sphere of water molecules, and subsequently deleting all water molecules except those with oxygens at least 2.5 Å away from the complex. After hydration, water molecules located more than 4.5 Å away from the complex were removed. A total of 632 water molecules were used for the hydration. The geometry of the hydrated complex was then energy minimized by CHARMM [24] using an all-atom parameter set [34]. The hydrated complex with a harmonic positional restraint $k = 1.0$ on AR–NADPH–Crystal H_2Os–D-glyceraldehyde was minimized for the first 1000 steps with the steepest descent method to allow the water molecules to optimize relative to the protein. The hydrated complex was then further minimized without restraints using the adopted basis Newton–Raphson (ABNR) method until the energy gradient fell below 0.01 kcal mol^{-1} Å^{-1}. Energy minimizations were performed with a constant dielectric constant ($\varepsilon = 1$). Electrostatic force was treated with the force switch method [35] and a switching range of 8–12 Å for MM interactions and without cutoffs for QM/MM electrostatic interactions. Van der Waals forces were calculated with the shift method with a cutoff of 12 Å. All calculations by CHARMM or GAMESS/CHARMM were performed on a cluster of HP-735 workstations.

Using the geometry of the hydrated complex minimized by CHARMM as a starting point, the active site of AR was partitioned into QM and MM regions as illustrated in Fig. 2. The QM region consisted of the phenol ring of Tyr48, imidazoline ring of His110, nicotinamide ring of the NADPH and a portion of D-glyceraldehyde as well as the carboxylate of Asp43 and a portion of Lys77. All other atoms outside the QM region were assigned to the MM region. Each of the QM portions was connected to MM region through a link atom hydrogen as denoted by the asterisks in Fig. 2. After partitioning the active site of AR into the QM and MM regions, the geometry of the hydrated complex was further minimized with ABNR by GAMESS/CHARMM while treating atoms in the QM region quantum mechanically with the 4-31G basis set. Atoms located more than 12 Å away from the phenylhydroxyl oxygen of Tyr48 were fixed in space during the QM/MM energy minimization since the geometry of QM region was expected to be only minimally affected by these distantly located MM atoms. In the QM/MM energy minimization, electrostatic interactions between QM atoms and MM atoms in the group [25] containing link atoms were excluded utilizing the 'exgr' option so that MM atoms interacted with the QM region primarily as a neutral electrostatic group. Geometry optimizations by GAMESS/CHARMM were carried out with protonated His110 as well as with neutral His110 with a hydrogen on the $N\varepsilon 2$ atom. QM/MM energy minimization was terminated when the energy change for the last five cycles became less than 0.8 kcal/mol. This required 40 to 60 cycles of QM/MM energy minimization. The RMS gradient for each of the QM/MM optimized structures was less than 0.6 kcal mol^{-1} Å^{-1}.

2.3. Proton and hydride transfer utilizing restrained distance method

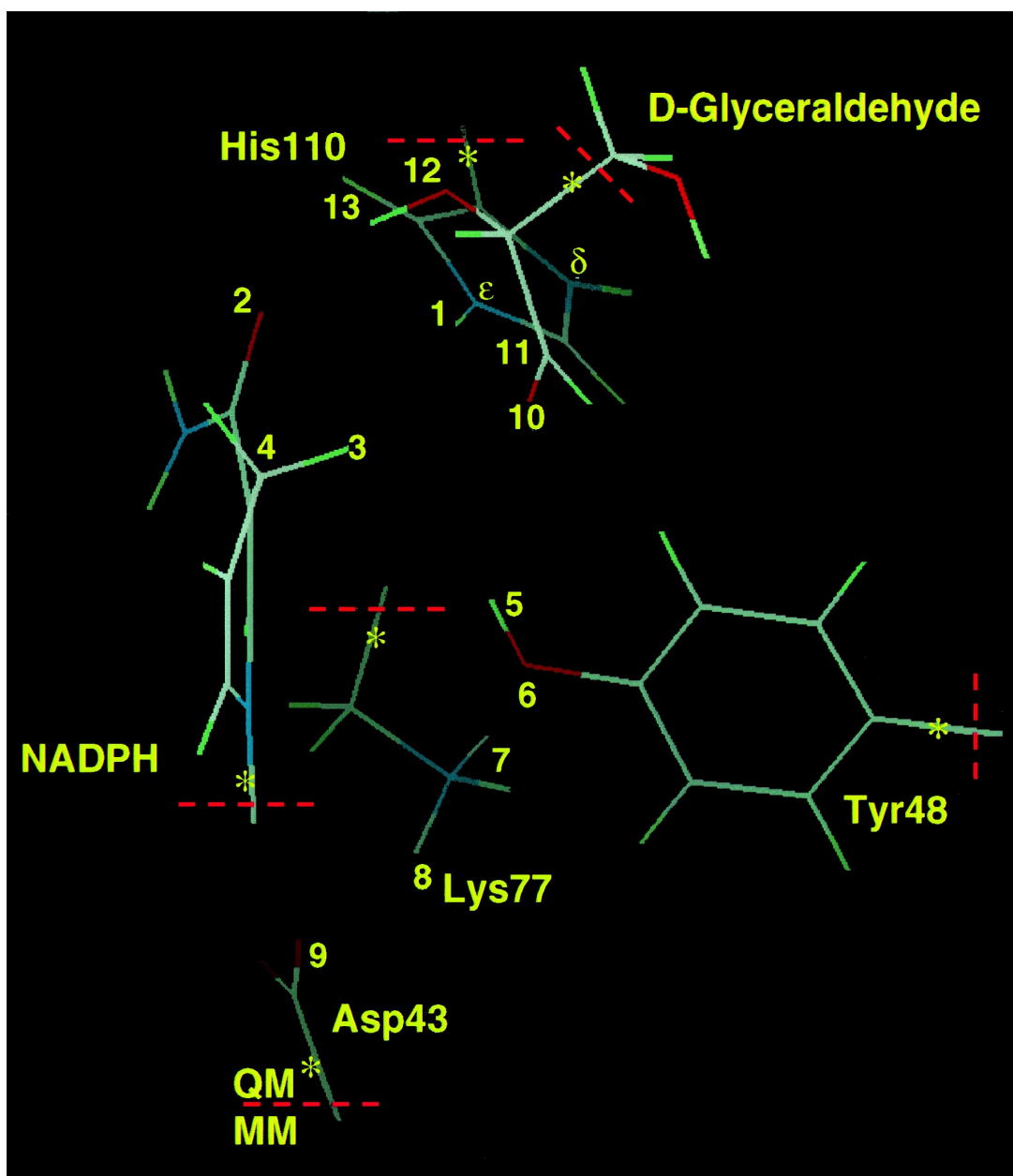After obtaining the QM/MM optimized geometries of D-glyceraldehyde at the active site, the hy-

Fig. 2. The active site of human aldose reductase with the QM/MM partition. Shown is the active site of aldose reductase with substrate D-glyceraldehyde after energy minimization by CHARMM. The active site was partitioned into QM and MM regions as indicated by dotted lines. Each of the QM portions was connected to the MM region through a link atom hydrogen as denoted by [*]. Atoms were numbered to specify the distance between two atoms.

dride of NADPH and the proton of His110 or Tyr48 were moved to the substrate carbonyl oxygen to construct the potential energy surface of the reduc-

tion process utilizing the restrained distance (RESD) method, which is used to restrain a general linear combination of distances. Fig. 3 depicts a potential
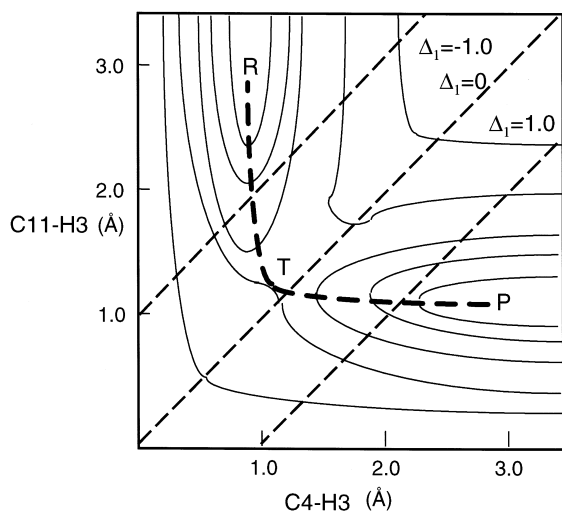
Fig. 3. A schematic diagram depicting the use of the RESD method in locating a minimum energy pathway for the hydride transfer from the C4 atom of NADPH to the substrate carbonyl. The RESD method scans the potential energy surface along a contour where r_1 and r_2 are linearly related. R, T and P represent reactant, transition state and product, respectively. The minimum energy pathway as indicated by thick dotted lines can be located by an incremental variation of Δ_1 from the reactant side to product followed by energy minimization.

energy surface for the hydride transfer from the C4 atom of NADPH to the substrate carbonyl. To locate a minimum energy pathway for the hydride transfer as indicated by the dotted line, a harmonic restraint energy term for hydride $E_{res}(H^-) = k/2\,(r_1 - r_2 - \Delta_1)^2$ was included in energy minimization process where k is a force constant, and r_1 and r_2 are the distance of C4–H3, and H3–C11, respectively (see Fig. 2 for number assignment on atoms); Δ_1 is a variable parameter, the difference between r_1 and r_2. The RESD method scans the potential energy surface along a contour where r_1 and r_2 are linearly related. Thus, the transition state on the minimum energy pathway shown in Fig. 3 can be located by an incremental variation of Δ_1 from the reactant side to the product followed by energy minimization. Since the reduction process involves the movement of both hydride and proton, a harmonic restraint energy term for proton $E_{res}(H^+) = k/2\,(r_3 - r_4 - \Delta_2)^2$ was also included in the energy minimization process where r_3 and r_4 represent the distance of Nε2–H1 and H1–O10, respectively when His110 was treated as

the proton donor, and r_3 and r_4 represent the respective distance of O6–H5 and H5–O10 when Tyr48 was treated as the proton donor. The force constant k in both equations was set to a large value (1500 kcal mol^{-1} Å^{-2}) during energy minimization. The QM/MM optimized geometries with protonated His110 and neutral His110 were utilized for the reaction catalyzed by His110 and Tyr48, respectively.

For the reduction process catalyzed by His110, the hydride was moved from the C4 of NADPH to the substrate carbonyl carbon by varying Δ_1 from -1.5 to 1.5 Å with an increment of 0.5 Å while the Nε2 hydrogen of His110 was moved to the substrate carbonyl oxygen by varying Δ_2 from -1.0 to 1.0 Å with an increment of 0.5 Å. For the reduction process catalyzed by Tyr48, the hydride was moved in the above-mentioned manner while the hydroxyl hydrogen of Tyr48 was moved to the substrate carbonyl oxygen by varying Δ_2 from -1.5 to 1.0 Å with an increment of 0.5 Å. The QM/MM energy minimization with RESD was carried out by excluding electrostatic interactions between QM atoms and six MM atoms connected to link atom hydrogen. The 3′-hydroxyl oxygen of D-glyceraldehyde as well as the oxygen atom (O4N) on the ribose ring of NADPH were also excluded from interacting with QM atoms to prevent the shift of the link atom hydrogens toward these oxygen atoms. All energy minimization with RESD were terminated when the energy change for the last five cycles became less than 1.0 kcal/mol. This required 25 to 30 cycles of energy minimization on each grid point.

3. Results

3.1. Binding mode of D-glyceraldehyde at the active site of AR

The 4-31G optimized geometry of QM atoms illustrates a spatial position of D-glyceraldehyde substrate at the active site prior to catalysis (Fig. 4). Protonated His110 forms a hydrogen bond with the amide oxygen of NADPH as well as with the carbonyl and 2′-OH of D-glyceraldehyde. Tyr48 is hydrogen bonded to both the substrate carbonyl and
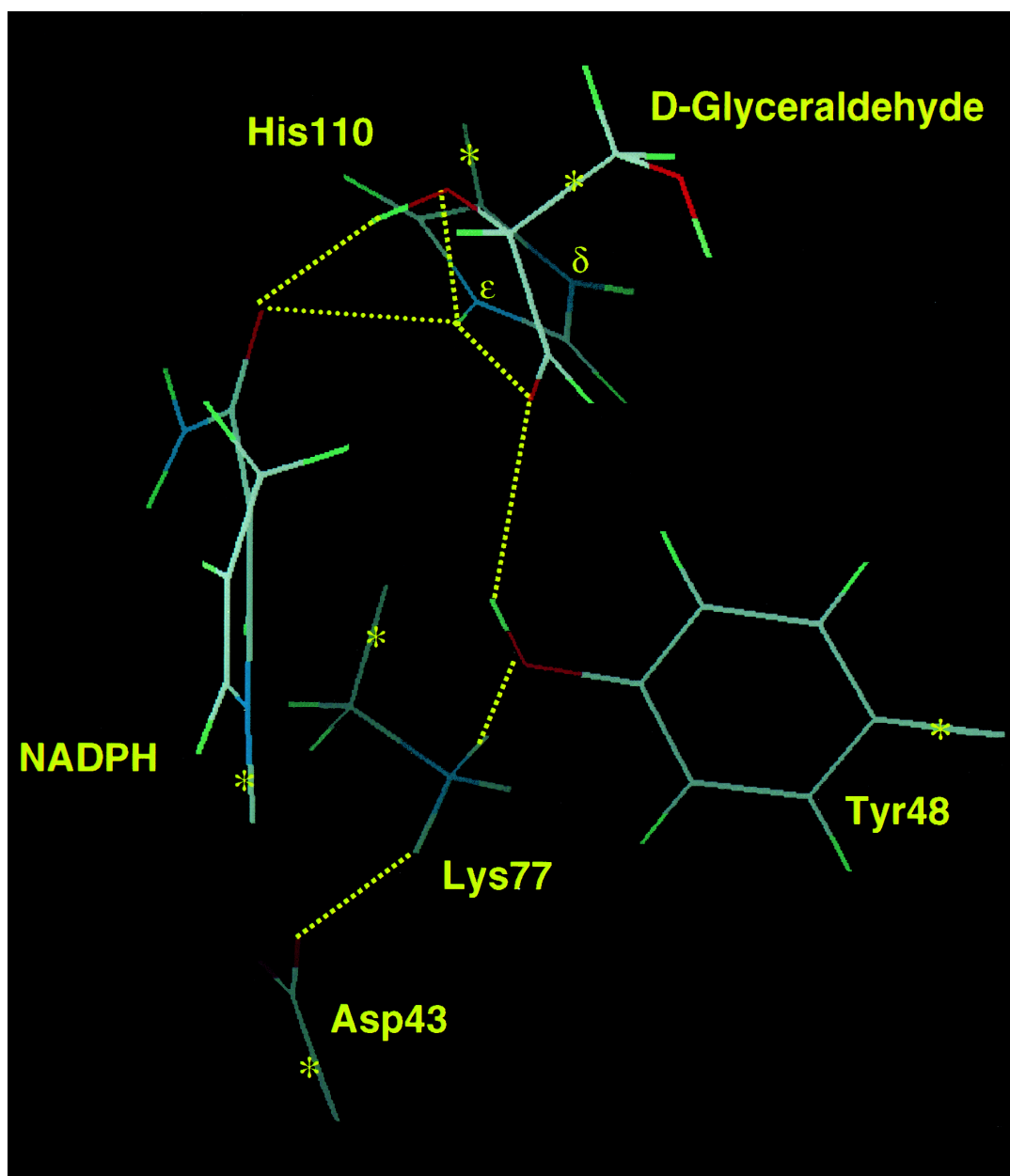
Fig. 4. The QM/MM optimized geometry of the active site of human aldose reductase. Dotted lines indicate the 4-31G optimized hydrogen bond distances (< 2.55 Å) among the QM atoms at the active site of AR.

Lys77. The optimized structure indicates that the substrate carbonyl is properly positioned in the active site to accept the *4-pro-R* hydrogen of NADPH and a proton from either Tyr48 or His110 during catalysis. The *4-pro-R* hydrogen of NADPH is located 2.60 Å away from the substrate carbonyl carbon while the Nε2 hydrogen of His110 and the hydroxyl hydrogen of Tyr48 are located 1.95 and

Table 1
QM/MM optimized hydrogen bond distances (Å) between QM atoms in the active site

	H1–O2	H1–O10	H5–O10	H7–O6	H8–O9	H13–O2	H1–O12
His$^+$110	2.37	1.95	2.55	1.81	1.71	1.86	2.36
His110[a]	2.53	2.05	2.43	1.80	1.73	1.87	2.26

[a] H on the $N\varepsilon 2$ atom.

2.55 Å away from the substrate carbonyl oxygen, respectively. The 4-31G optimized structure also shows that Asp43, Lys77 and Tyr48 form a hydrogen bonding network as observed in the crystal structures of AR [4,5,16]: Asp43 is salt-linked with Lys77 (1.71 Å) and Lys77 in turn forms a strong hydrogen bond (1.81 Å) with the hydroxyl of Tyr48. A similar hydrogen bonding pattern, illustrated in Fig. 4, is observed in the optimized geometry with neutral His110 (hydrogen on the $N\varepsilon 2$). The optimized hydrogen bond distances between the QM atoms at the active site are summarized in Table 1.

Proper hydrogen bonding interactions depicted in Fig. 4 are not obtained by the STO-3G optimized geometry of QM atoms. For example, the STO-3G optimized geometry favors a neutral complex between Asp43 and Lys77 rather than an ionic one. Accordingly, a split-valence basis set (4-31G) was used in our studies to adequately describe hydrogen bonding interactions in the protein environment [36].

3.2. Reduction process catalyzed by His110 or Tyr48

The potential energy surfaces for the reduction of D-glyceraldehyde to glycerol constructed with His110 and Tyr48 as the proton donor are illustrated in Figs. 5 and 6, respectively. Dotted lines on the potential energy surface indicate a minimum energy pathway for each of the reduction processes. After locating a transition state on the potential energy surface, further energy minimizations on the geometry of the reactant, transition state and product were carried out until the energy change became less than 0.2 kcal/mol for the last 10 cycles. The resulting geometries and energetics at the reactant, transitions state and product are shown in Figs. 7 and 8. In both cases, the substrate carbonyl is hydrogen bonded to His110 and Tyr48 in the reactant stage. The transition state geometry for the reaction catalyzed by His110 is characterized by a halfway transfer of
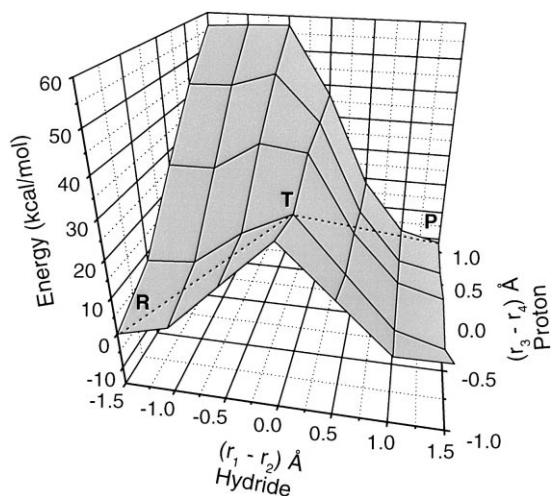

Fig. 5. The potential energy surface for the reduction process catalyzed by His110.
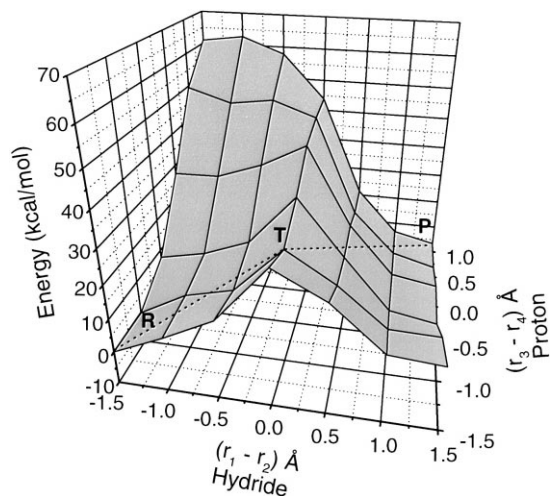

Fig. 6. The potential energy surface for the reduction process catalyzed by Tyr48.

hydride from NADPH and a partial transfer of the proton from His110 to the substrate carbonyl. The transition state geometry for the reaction catalyzed by Tyr48 displays a halfway transfer of hydride from NADPH and essentially no proton transfer from Tyr48 to the substrate carbonyl. The product stage displays the formation of $NADP^+$ and the product glycerol.
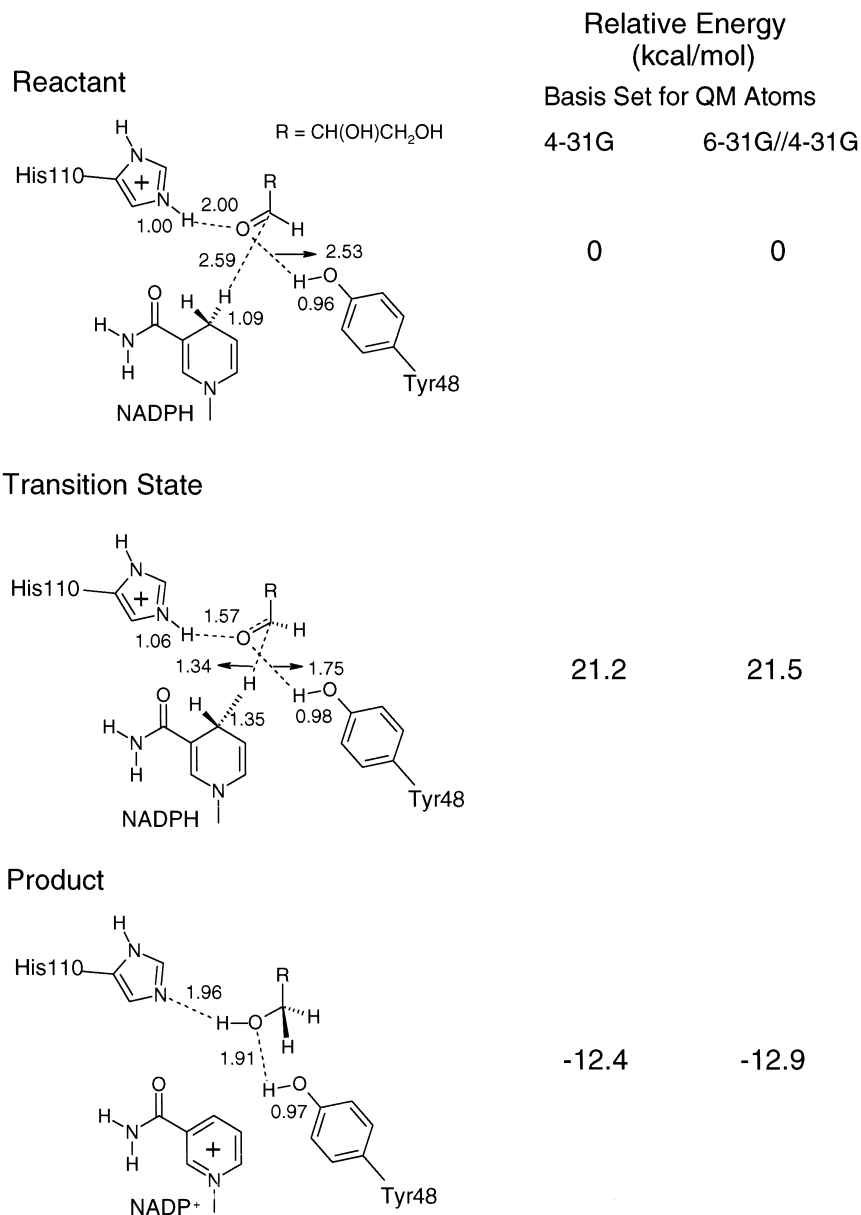

Fig. 7. The geometry and energies of the reactant, transition state and product with His110 as the proton donor.

In order to see the effect of the basis set on the energetics, single point calculations with the 6-31G basis set on the three states defined in Figs. 7 and 8 were calculated. Single point calculations with the 4-31G basis set were also carried out on the three states on QM atoms as defined in Fig. 2 to compare
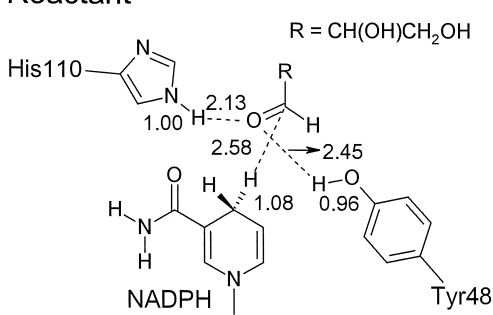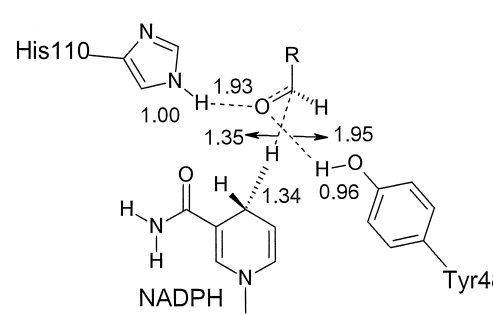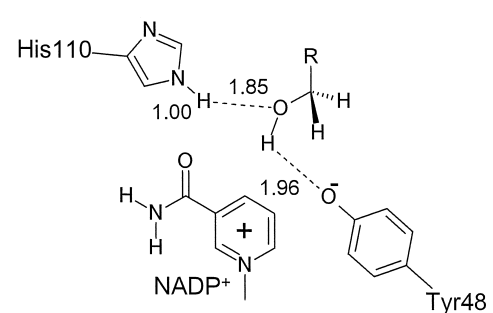

Fig. 8. The geometry and energetics of the reactant, transition state and product with Tyr48 as the proton donor.

Table 2
Relative energetics (kcal/mol) of the two reduction processes

	Proton donor			
	His110		Tyr48	
	QM	QM/MM	QM	QM/MM
E_a	25.9	21.2	34.4	24.3
ΔH	−3.9	−12.4	14.5	−3.7

the energetics between QM and QM/MM calculations (Table 2).

4. Discussion

4.1. Protonation state of His110

Multiple hydrogen bonding interactions shown in Fig. 4 indicate that the complex of AR–NADPH recognizes substrate D-glyceraldehyde mainly through hydrogen bonding. These hydrogen bonding interactions can provide important information in determining the protonation state of His110. It has been claimed that the hydrophobic environment lowers the pK_a of His110 at the active site of AR, thus favoring neutral His110 over the protonated one [4,7]. However, the crystal structure of murine aldoketo reductase and human AR complexed with the inhibitor zopolrestat [20,21] reveals that the Nε2 hydrogen of His110 is salt-linked to the carboxyl anion of zopolrestat, assuring that His110 is protonated even in a hydrophobic environment. His110 while remaining neutral during catalysis could become protonated because of the interaction between the Nε2 hydrogen and the carboxylate of zopolrestat. However, the present QM/MM optimized structure clearly demonstrates that the Nε2 hydrogen of His110 can be hydrogen bonded to the amide oxygen of NADPH as well as to the carbonyl and 2′-OH of D-glyceraldehyde. In addition to these three hydrogen bonding interactions with the Nε2 hydrogen of His110, a water channel in the crystal structure provides an additional hydrogen bond to the Nδ1 hydrogen of His 110. These multiple hydrogen bonding interactions are expected to stabilize the protonated form of His110.

Observations that Trp residues at the active site of proteins tend to stabilize the protonated from of His

[37,38] also supports the premise that His110 is protonated. For example, in a fluorescence quenching study, it has been demonstrated that Trp residue at the active site of barnase elevates the pK_a of a neighboring His to 7.75 through histidine–aromatic interactions [38]. Trp79 or Trp111 at the active site of AR, as illustrated in Fig. 1, may provide similar interactions to elevate the pK_a of His110.

4.2. Energetics

The shapes of the potential energy surfaces shown in Figs. 5 and 6 are very similar: the reduction process is heavily dictated by the hydride transfer no matter whether His110 or Tyr48 contributes the proton. The two potential energy surfaces illustrate that an initial proton transfer from either residue is not likely because of a steep increase in energy along the proton reaction coordinate. Proton transfer becomes energetically favorable only after the hydride transfer is more than halfway complete. Because of the positive charge on His110, proton transfer from His110 to the substrate carbonyl oxygen (O10–H1 = 1.57 Å) is more pronounced at the transition state compared to the proton transfer (O10–H5 = 1.95 Å) from Tyr48. Consequently, the E_a of the reduction process catalyzed by His110 is 3.1 kcal/mol lower than by Tyr48. In both cases (Figs. 7 and 8), Tyr48 and His110 seem to stabilize the transition state geometry through hydrogen bonding interactions. After crossing the transition state, the hydride and the proton appear to move in a concerted manner without a noticeable energy barrier to form the product glycerol. QM/MM calculations indicate that the reduction catalyzed by His110 is thermodynamically favorable by 8.7 kcal/mol over that catalyzed by Tyr48. This 8.7 kcal/mol difference in ΔH between the two reduction processes can be attributed to the formation of the tyrosinate anion. Although the tyrosinate anion can be stabilized by a neighboring Lys77 through electrostatic interaction, this interaction itself does not make the E_a or ΔH of the reaction catalyzed by Tyr48 comparable to that catalyzed by His110. A similar trend in energetics was observed when single point energy calculations with the 6-31G basis set were carried out on the states

defined in Figs. 7 and 8. The difference in energetics between the two basis sets is ≤ 0.5 kcal/mol indicating that the E_a and ΔH of the two reduction reactions are not much influenced by the size of a basis set.

The comparison of the E_a and ΔH from the QM and QM/MM calculations (Table 2) suggests that the protein environment makes the reduction process become more favorable both kinetically and thermodynamically. The E_a of the reaction catalyzed by His110 or Tyr48 in the protein environment is lower by 4.7 or 10.1 kcal/mol, respectively, than those from the QM calculations. The ΔH of the reaction catalyzed by His110 or Tyr48 in the protein environment is stabilized by 8.5 or 18.2 kcal/mol, respectively. The protein environment appears to greatly influence the energetics of the reduction process catalyzed by Tyr48. A more accurate description of the QM/MM interaction energies may answer whether the protein environment indeed influences the reaction catalyzed by Tyr48 more than the one catalyzed by His110. This is an area of active development and further methodological improvement will improve our ability to accurately calculate QM/MM interaction energies.

It is worth noting that the present reaction pathway study makes no estimate of entropic contributions and merely determines a reaction pathway based upon the potential energy. Since the two reduction processes differ by only one proton, the entropic contributions can be assumed to be similar in magnitude and most likely to be canceled out when comparing the energetics of the two reduction processes. The comparable curvatures of the saddle points illustrated in Figs. 5 and 6 support this premise, however, a further examination of the energetics of additional degrees of freedom that are orthogonal to the reaction pathway would be necessary to confirm this assumption.

4.3. Reaction mechanism

The present QM/MM calculations suggest that the reduction process is primarily determined by the hydride transfer regardless of the proton source, and this makes the energy barrier for the proton transfer negligible. This finding, however, is not in agreement with the solvent isotope study done on the wild type human AR. The primary deuterium and solvent isotope effect on k_{cat}/K_m for DL-glyceraldehyde reduction were reported to be 1.82 and 4.73, respectively [7]. Because of a larger solvent isotope effect on k_{cat}/K_m, it was proposed that proton transfer may contribute significantly more to the overall rate limitation of the catalytic process than does hydride transfer [7]. In contrast, the kinetic isotope study done on the Y48H mutant showed that the hydride transfer rather than the proton transfer is a slow step, which is in agreement with the present finding; either His48 or His110 at the active site of the Y48H mutant can be the source of the proton in the reduction process. In the Y48H mutant study [7], essentially no solvent isotope effect on k_{cat}/K_m was observed (1.06) while the primary isotope effect on k_{cat}/K_m was reported to be 1.81. Thus, the proton transfer is not a slow process compared to the hydride transfer.

If the reduction undergoes two discrete steps, hydride transfer along the hydride reaction coordinate and then the proton transfer along the proton reaction coordinate, there is ca. 1.1 kcal/mol energy barrier for the proton transfer from His110 and 1.5 kcal/mol from Tyr48 (Figs. 5 and 6). This 1.5 kcal/mol energy barrier is not likely to make the proton transfer process slower than the hydride transfer process even if the reduction undergoes two discrete steps with Tyr48 as the proton donor. It remains puzzling to explain the large deuterium isotope effect on k_{cat}/K_m for DL-glyceraldehyde reduction by human AR based on the potential energy surfaces shown in Figs. 5 and 6.

4.4. Catalytic activity of Tyr48 and His110 mutants

Our finding from the QM/MM calculations that the reduction of aldehyde substrate to alcohol by AR is energetically favorable with His110 as the proton donor may shed new light on the interpretation of the inactivity [7] or the three-fold decrease in catalytic efficiency [6] observed when Lys77 was mutated to methionine (K77M). Substitution of methionine for Lys77 severely disrupts the hydrogen bonding network that exists in the Asp43–Lys77–Tyr48 complex; the strong hydrogen bond (1.81 Å) between the positively charged amino group of Lys77 and the hydroxyl of Tyr48 is broken. As a result, the hy-

droxyl of Tyr48 in the K77M mutant may not be properly aligned to form a hydrogen bond to the substrate carbonyl oxygen, which, in turn, results in a large increase in K_m, and decrease in k_{cat} for aldehyde substrates (see Fig. 4). Similar reasoning can be invoked for the absence of activity in human AR [6,7] or a slight activity of rat lens AR [22] observed with DL-glyceraldehyde as substrate when Tyr48 was mutated to phenylalanine. Phenylalanine cannot form a hydrogen bond to either Lys77 or the substrate carbonyl oxygen, and this may give rise to very unfavorable orientation of the substrate carbonyl for catalysis. Both Lys77 and Tyr48 appear to be structurally critical residues for maintaining the integrity of the substrate binding site of AR.

Mutation of His110 does not result in abolished reductase activity. Residual activity remains with decrease of k_{cat}/K_m ranging from 10^3 to 10^6 fold compared with the k_{cat}/K_m of wild type human AR [6,7]. The observed residual activity of the His110 mutants of AR may well arise from Tyr48. Our calculation suggests that the reduction process catalyzed by Tyr48 is also a thermodynamically favorable process. Thus, Tyr48 can serve as the proton donor although not as effective as His110 in terms of catalytic efficiency. In other words, Tyr48 can step up as the proton donor in the absence of His110 at the active site of AR. This may account for the low activity of AR observed when His110 was mutated [6,7,22].

With the exception of Japanese bull frog ρ-crystalline, the catalytic site of the known aldo-keto reductase superfamily may represent a unique environment in which both His110 and Tyr48 form hydrogen bonds to the substrate carbonyl, and at the same time can act as proton donor. The issue is which residue is a better proton donor. The present work supports the experimental findings that His110 were suggested to be the proton donor in catalysis.

5. Summary

The water channel linking the Nδ1 hydrogen of His110 to the bulk solvent as well as hydrogen bonding interactions to the Nε2 hydrogen of His110 provided by the amide oxygen of NADPH and by the 2′-hydroxyl and the carbonyl of D-glyceraldehyde

are suggested to stabilize the protonated form of His110. The reduction of D-glyceraldehyde to glycerol catalyzed by His110 is both kinetically and thermodynamically favorable over the reduction process catalyzed by Tyr48. The reduction of D-glyceraldehyde catalyzed by AR is dictated by the hydride transfer up to the transition state. After passing the transition state, both the proton and the hydride move in a concerted manner to form product glycerol. Tyr48 appears to be a structurally critical residue together with Lys77 for preserving the integrity of the substrate binding site of AR. The loss of the catalytic activity of the Y48F and the K77M mutant of AR is attributed to the disruption of a hydrogen bonding network in the Asp43–Lys77–Tyr48 complex while the residual activity of the His110 mutants of AR is ascribed to Tyr48.

Acknowledgements

References

[1] J.H. Kinoshita, Am. J. Ophthalmol. 102 (1986) 685.
[2] P.F. Kador, Med. Res. Rev. 8 (1988) 325.
[3] J.M. Rondeau, F. Tete-Favier, A. Podjarny, J.M. Reymann, P. Barth, J.F. Biellmann, D. Moras, Nature 355 (1992) 469.
[4] D.K. Wilson, K.M. Bohren, K.H. Gabbay, F.A. Quiocho, Science 257 (1992) 81.
[5] D.H. Harrison, K.M. Bohren, D. Ringe, G.A. Petsko, K.H. Gabbay, Biochemistry 33 (1994) 2011.
[6] I. Tarle, D.W. Bohrani, D.K. Wilson, F.A. Quiocho, J.M. Petrash, J. Biol. Chem. 268 (1993) 25687.
[7] K.M. Bohren, C.E. Grimshaw, C.J. Lai, D.H. Harrison, D. Ringe, G.A. Petsko, K.H. Gabbay, Biochemistry 33 (1994) 2021.
[8] J.M. Petrash, T.M. Harter, C.S. Devine, P.O. Olins, A. Bhatnagar, S.Q. Liu, S.K. Srivastava, J. Biol. Chem. 267 (1992) 24833.
[9] C.E. Grimshaw, K.M. Bohren, C.J. Lai, K.H. Gabbay, Biochemistry 34 (1995) 14356.
[10] C.E. Grimshaw, K.M. Bohren, C.J. Lai, K.H. Gabbay, Biochemistry 34 (1995) 14366.
[11] C.E. Grimshaw, K.M. Bohren, C.J. Lai, K.H. Gabbay, Biochemistry 34 (1995) 14374.
[12] J.M. Petrash, I. Tarle, D.K. Wilson, F.A. Quiocho, Diabetes 43 (1994) 955.
[13] H.L. De Winter, M.V. Itzstein, Biochemistry 34 (1995) 8299.

[14] S.Q. Liu, A. Bhatnagar, S.K. Srivastava, J. Biol. Chem. 268 (1993) 25494.

[15] S.Q. Liu, A. Bhatnagar, N.H. Ansari, S.K. Srivastava, FASEB J. 8 (1994) A936.

[16] F. Tete-Favier, P. Bath, A. Mitchler, A.D. Podjarny, J.M. Rondeau, A. Urzhumtsev, J.F. Bielmann, Euro. J. Med. Chem. 30 (1995) Suppl: 589s.

[17] J.E. Pawlowski, T.M. Penning, J. Biol. Chem. 269 (1994) 13502.

[18] O. El-Kabbani, K. Judge, S.L. Ginell, D.A. Myles, L.J. Delucas, T.G. Flynn, Nature Struct. Biol. 2 (1995) 687.

[19] O.A. Barski, K.H. Gabbay, C.E. Grimshaw, K.M. Bohren, Biochemistry 34 (1995) 11264.

[20] D.K. Wilson, I. Tarle, J.M. Petrash, F.A Quiocho, Proc. Natl. Acad. Sci. USA 90 (1993) 9847.

[21] D.K. Wilson, T. Nakano, J.M. Petrash, F.A. Quiocho, Biochemistry 34 (1995) 14323.

[22] A.D. Carper, T.C. Hohman, S.E. Old, Biochim. Biophys. Acta 1246 (1995) 67.

[23] M.W. Schmidt, K.K. Baldridge, J.A. Boatz, S.T. Elbert, M.S. Gordon, J.J. Jensen, S. Koseki, N. Matsunaga, K.A. Nguyen, S. Su, T.L. Windus, M. Dupuis, J.A. Montgomery, J. Comput. Chem. 14 (1993) 1347.

[24] B.R. Brooks, R.E. Bruccoleri, B.D. Olafson, D.J. States, S. Swaminathan, M. Karplus, J. Comput. Chem. 4 (1983) 187.

[25] K.P. Eurenius, D.C. Chatfield, M. Hodoscek, B.R. Brooks, Int. J. Quantum Chem. 60 (1996) 1189.

[26] A. Warshel, M. Levitt, J. Mol. Biol. 103 (1976) 227.

[27] P.A. Bash, M.J. Field, R.C. Davenport, G.A. Petsko, D. Ringe, M. Karplus, Biochemistry 30 (1991) 5826.

[28] D.S. Hartsough, K.M. Mertz, J. Phys. Chem. 99 (1995) 11266.

[29] V.V. Vasilyev, J. Mol. Struc. (Theochem.) 304 (1994) 129.

[30] M.J. Field, P.A. Bash, M. Karplus, J. Comput. Chem. 11 (1990) 700.

[31] U.C. Singh, P.A. Kollman, J. Comput. Chem. 7 (1986) 718.

[32] J. Gao, J. Phys. Chem. 96 (1992) 537.

[33] M.J. Frisch, G.W. Trucks, H.B. Schlegel, P.M.W. Gill, B.G. Johnson, M.A. Robb, J.R. Cheeseman, T. Keith, G.A. Petersson, J.A. Montgomery, K. Raghavachari, M.A. Al-Laham, V.G. Zakrzewski, J.V. Ortiz, J.B. Foresman, J. Cioslowski, B.B Stefanov, A. Nanayakkara, M. Challacombe, C.Y. Peng, Y. Ayala, W. Chen, M.W. Wong, J.L. Andres, E.S. Replogle, R. Gomperts, R.L. Martin, D.J. Fox, J.S. Binkley, D.J. Defrees, J. Baker, J.P. Stewart, M. Head-Gordon, C. Gonzalez, J.A. Pople, Gaussian 94, Revision C.2, Gaussian, Pittsburgh, PA, 1995.

[34] Molecular Simulation, Parameter file for CHARMm Version 22 (1992), Waltham, MA.

[35] P.J. Steinbach, B.R. Brooks, J. Comput. Chem. 15 (1994) 667.

[36] M. Hodoscek, D. Hadzi, J. Mol. Struct. 198 (1989) 461.

[37] R. Lowenthal, J. Sancho, A.R. Fersht, Biochemistry 30 (1991) 6775.

[38] R. Lowenthal, J. Sancho, A.R. Fersht, J. Mol. Biol. 224 (1992) 759.